Heliyon 10 (2024) e26958

Contents lists available at ScienceDirect

Heliyon

journal homepage: www.cell.com/heliyon

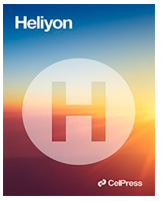

Research article

Cross-diffusive flow of MHD micropolar nanofluid past a slip stretching plate

Xiyan Tian [a,b,*], Bingbing Yang [a,b], Xin Na [c], Liankang Ba [a,b], Yi Yuan [a,b]

[a] Key Laboratory of National Education Ministry for Electromagnetic Processing of Materials, POB 314, Northeastern University, Shenyang 110819, China
[b] School of Metallurgy, POB 314, Northeastern University, Shenyang 110819, China
[c] Department of Information and Control Engineering, Shenyang Urban Construction University, Shenyang 110167, China

ARTICLE INFO

Keywords:
MHD micropolar nanofluid
First order slip
Boundary layer
Cross-diffusion
Viscous dissipation
Collocation spectral method (CSM)

ABSTRACT

As a novel fluid of functional material, magnetohydrodynamic (MHD) micropolar fluid has the special properties of light, heat, magnetic and so on. It is of highly practical significance. The characteristics of flow, heat and mass transfer in MHD micropolar nanofluid boundary layer past a stretching plate are investigated based on the micropolar fluid theory in the present numerical work. In the presence of magnetic field, viscous dissipation and the cross-diffusion caused by Dufour effect and Soret effect are considered. First order slip velocity condition is employed. Mathematical models are built based on the assumptions. Collocation spectral method (CSM) via matrix multiplication is adopted to solve the two-dimensional dimensionless nonlinear partial governing equations. The program codes based on CSM is developed, validated and employed. The coupled effects of microrotation, Dufour effect, Soret effect, magnetic field as well as first order slip velocity boundary condition on the flow, heat and mass transfer are revealed. Besides, the variation trends of local Nusselt number and Sherwood number are analyzed in detail. The numerical results indicate that the fluid flow can be suppressed obviously in the consideration n of slip condition and magnetic field. As slip parameter δ and magnetic parameter M rise, the velocity in the boundary layer becomes lower gradually; further, both temperature and concentration increase. On the other hand, the opposite trend can be noticed with the effect of material parameter K. Moreover, Ec and Df augment the temperature; while, Sr leads to an upsurge in concentration. The temperature rises by about 79.73% with Dufour effect and Sh enlarges by a factor of about 38.15% with Soret effect. The concentration boundary layer decreases by about 37.50% is when $K = 5.0$.

1. Introduction

Micropolar fluid (MF) proposed by Eringen [1], is a typical non-Newtonian fluid, such as human blood, liquid battery, lubricant, liquid crystal, polymer fluid and so on. Different from classical Newtonian fluid, MF presents the nature of micro inertia and micro rotation characteristics because of its asymmetrical structure. It is common to take MHD MF as working medium in the practical industry application, transportation, medicine and other fields, such as safety valves, shock absorbers, suspension systems, magnetic

* Corresponding author. Key Laboratory of National Education Ministry for Electromagnetic Processing of Materials, POB 314, Northeastern University, Shenyang 110819, China.
E-mail address: tianxy@epm.neu.edu.cn (X. Tian).

https://doi.org/10.1016/j.heliyon.2024.e26958
Received 27 September 2023; Received in revised form 20 February 2024; Accepted 22 February 2024
Available online 28 February 2024

seals, drug delivery, etc. The transport phenomenon of MF cannot be analyzed by hydrodynamic theory of classical continuous fluid through Navier-Stokes equation (*N*–S equation), since the stress tensor is treated to be symmetrical in the *N*–S model, and the influence of molecular spin can't be considered [2,3]. Hogan and Henriksen [4] studied the ideal blood flow; they found that although the resultant velocity and streamline via the classical continuous theory were similar to those via the micropolar continuous model theory, the discrepancy of shear stress was as high as 50%. To address the issues above, MF theory is preferred to reveal the influence of microparticles on base fluid; moreover, the application of classical theories of continuous model mechanics is expanded [5].

It is worth noting that the sizes of micropolar particles are in nanometer scale. Thermal performance of the base fluid can be upgraded by dispersion of nano-sized micropolar particles. As a result, MF presents the similar superior properties as nanofluid does, such as superior heat transfer rate and high thermal efficiency [6,7]. The conductivity of the base fluid may change significantly. With the wide applications of MF in the new energy storage and the traditional industrial fields, the topic of MF has received high consideration in recent years [8–23]. Under the action of magnetic field, fluid flow can be controlled; further, heat and mass transfer can be affected indirectly [24–28]. Salawu et al. [29] investigated that Lorentz force suppressed the movement of micropolar particles while strengthened the liquid binding effect, hence inhibited the velocity field. Recently, the flow features of MF with radiation and viscous effect is studied by Kumar et al. [30]. They concluded that the friction coefficient was inversely proportional to the magnetic field parameter. Mabood et al. [31] gave an analytical solution of the unsteady nanofluid flow through a convective heating surface with the action of Lorentz force, and obtained that the magnetic field tended to enhance the thermal function curve [32]. The effects of Hall current and radiation absorption on magnetohydrodynamic (MHD) MF in a rotating system is discussed by Narayana. Waqas et al. [33] applied convective conditions to MHD MF and calculated the surface friction coefficient and heat transfer rate. The research of radiative flow of MHD micropolar nanofluids past a nonlinear tensile surface was carried by Lu et al. [34], with both homogeneous and heterogeneous reactions.

With the fixed temperature gradient, thermal diffusibility of molecules or microparticles due to concentration difference is heterogeneous in micropolar nanofluid, which resulted in the directional migration of microparticles. It is so called Soret effect. On the contrary, the concentration diffusion caused by the temperature gradient is Dufour effect. Finally, the dynamic equilibrium can be achieved as a result of the interaction of concentration diffusion with temperature gradient and temperature diffusion with concentration gradient. Some scholars believe that the influence of the cross-diffusion effect (Dufour-Soret effect) is much smaller than that described by Fourier's law and Fick's law, which can be treated as a second-order phenomenon and can be ignored. In fact, Soret-Dufour effect cannot be underestimated especially in some natural convection or in the case of large temperature and concentration gradients; even, in some mixed fluid systems with weak flow or thermal boundary with small disturbance, Dufour effect has a strengthening influence on heat transfer significantly. Reddy et al. [35,36] studied Dufour-Soret effects on flow and heat transfer of MF over a nonlinear porous stretching plate and confirm the abovementioned. Nowadays, more and more application of nanofluid behavior with cross-diffusive phenomena can be found in various industrial and high-tech fields [37–39]. Recently, due to the significance of flow and heat transfer on thin needle in many industry and engineering applications, mathematical research on convective heat transfer in non-Newtonian nanofluid's flow over a thin needle was carried out by Hassan et al. [40].

For some polymer solutions, the effect of slip boundary conditions cannot be ignored. Navier [41] first introduced the linear velocity slip boundary condition into the study of fluid flow. Later, Maxwell [42] revealed that the velocity slip boundary condition in the study of stress was caused by temperature difference in rarefied gas. Until now, as a classical problem, the topic of fluid flow with velocity slip boundary condition has drowned a strong attraction to the majority of researchers [43–49]. The partial slip effect of rotating disk on MHD micropolar nanofluids is analyzed by Ramzan et al. [50]. Nadeem et al. [51] studied the effect of micro rotation factors on heat transfer rate and microbial flora distribution with the slip boundary conditions. In the consideration of nonlinear radiation, the effects of variable viscosity and thermal conductivity on MHD Casson nanofluid boundary layer flow is discussed by Gbadeyan et al. [52], with convective heating slip boundary condition. Flow characteristics of MF caused by nonlinear surface with viscous dissipation were investigated by Ahmad et al. [53]. Fatunmbi et al. [54] studied the boundary layer flow of MF with variable physical properties and found that entropy production S rose as Prandtl number (Pr) and Eckert number (Ec) increased; heat transfer enhanced by viscous dissipation. Furthermore, Bejan number (Be) was observed to decrease with the increasing irreversibility caused by Joule heating.

To sum up, heat and mass transfer characteristics of MF are affected by many influential factors such as slip velocity boundary conditions, cross-diffusion effect and physical natures of micropolar particles. It is noticeable that the couple effects of various factors such as magnetic field, Dufour effect and Soret effect, first order slip velocity boundary condition on the MHD MF cannot be simply linear superimposing, especially taking viscous dissipation into account. In this study, we focus on the flow, heat and mass transfer of MHD micropolar nanofluids through a stretching flat surface with magnetic field, attempting to reveal the law behind the physical phenomena. Viscous dissipation and Dufour-Soret effect caused by cross diffusion are taken into account. Based on this assumption, we set up original governing partial differential equations (PDEs) for the certain boundary layer problem. Different from common numerical method used in boundary layer problem (Runge-Kutta method (*R*–K method), finite volume method, finite element method, etc.) and the strategy of self-similar transformation, collocation spectral method (CSM) via matrix multiplication (MM) which is uncommon while highly accurate is utilized. We solve the 2D mathematical model instead of the quasi 1D model of self-similar transformation. The program code is developed accordingly. In consequence, the irregular variation trends and resultant physical phenomena can be discovered and studied.

2. Description of problem

As presented in Fig. 1, x and y axes are parallel and perpendicular to the stretching plate, respectively. The stretching speed of the

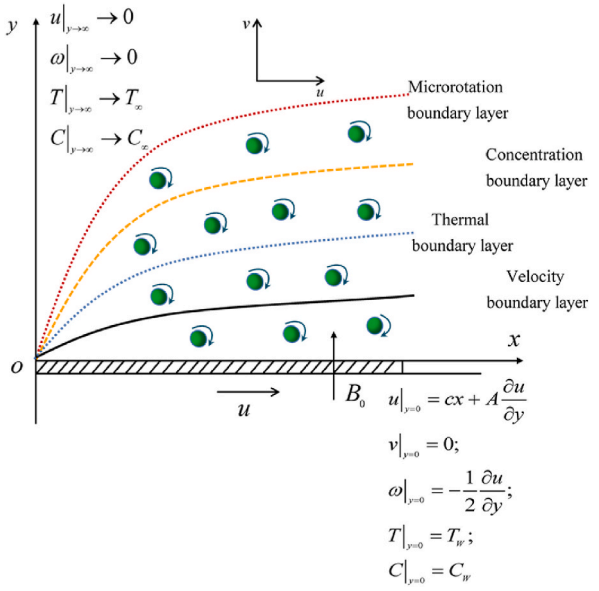

Fig. 1. The physical model.

plate is cx. A steady magnetic field B_0 is applied perpendicular to the plane. A thin boundary layer of MHD micropolar nanofluid forms along the wall. The temperature of fluid at the plate boundary is T_w and the concentration is C_w. It is noticed that $T_\infty < T_f < T_W$, $C_\infty < C_f < C_W$.

2.1. Basic assumptions

It is assumed that the angular velocity ω is perpendicular to the $x-y$ plane. Dufour effect and Soret effect caused by the cross diffusion, along with viscous dissipation are taken into account. Magnetic Reynolds number is so small that the induced magnetic field and thus the Hall effects can be ignored.

2.2. Mathematical model

According to the above basic assumptions, the original 2-D boundary layer governing equations of MHD micropolar nanofluid are obtained. Equations of mass conservation, linear momentum, angular momentum, energy and solutal concentration conservation are as following:

$$\frac{\partial u}{\partial x}+\frac{\partial v}{\partial y}=0 \tag{1}$$

$$u\frac{\partial u}{\partial x}+v\frac{\partial u}{\partial y}=\left(\frac{\mu_f+\mu_r}{\rho_f}\right)\frac{\partial^2 u}{\partial y^2}+\frac{\mu_r}{\rho_f}\frac{\partial \omega}{\partial y}-\frac{\sigma B_0^2}{\rho_f}u \tag{2}$$

$$u\frac{\partial \omega}{\partial x}+v\frac{\partial \omega}{\partial y}=\frac{\gamma}{\rho_f j}\frac{\partial^2 \omega}{\partial y^2}-\frac{\mu_r}{\rho_f j}\left(2\omega+\frac{\partial u}{\partial y}\right) \tag{3}$$

$$u\frac{\partial T}{\partial x}+v\frac{\partial T}{\partial y}=\frac{k}{\rho_f c_p}\frac{\partial^2 T}{\partial y^2}+\frac{D_m k_T}{c_s c_p}\frac{\partial^2 C}{\partial y^2}+\left(\frac{\mu_f+\mu_r}{\rho_f c_p}\right)\left(\frac{\partial u}{\partial y}\right)^2 \tag{4}$$

$$u\frac{\partial C}{\partial x}+v\frac{\partial C}{\partial y}=D_m\frac{\partial^2 C}{\partial y^2}+\frac{D_m k_T}{T_m}\frac{\partial^2 T}{\partial y^2} \tag{5}$$

The last term of Eq. (5) represents the contribution of Soret effect. u and v are linear velocity components in x and y directions, respectively; ω is angular velocity, T and C are temperature and concentration, respectively. μ_f is dynamic viscosity, μ_r is vortex viscosity, γ is spin-gradient viscosity, $j=\left(\frac{u_\infty^{n-2}\mu_f x}{\rho}\right)^{n+1}$ is micro-inertial density, σ is conductivity, B_0 is magnetic field strength, c_p is specific heat capacity at constant pressure, $D_m=\frac{\kappa}{\rho_f}$ is mass diffusion coefficient of the fluid.

The corresponding boundary conditions are:

$$u = cx + A\frac{\partial u}{\partial y}, v = 0, \omega = -\frac{1}{2}\frac{\partial u}{\partial y}, T = T_w, C = C_w \text{ on } y = 0\ u \to 0, N \to 0, T \to T_\infty, C \to C_\infty \text{ at } y \to \infty \tag{6}$$

where, c is a constant, A is first-order slip coefficient; T_W, C_W and T_∞, C_∞ are temperatures and concentrations on the wall boundary and in the ambient fluid, respectively.

In order to convert the above governing equations into the dimensionless ones, the following dimensionless variables are introduced:

$$X = \frac{x}{l}, Y = \frac{y}{l}Re^{1/2}, U = \frac{u}{U_\infty}, V = \frac{v}{U_\infty}Re^{1/2}, \omega = \frac{U_\infty}{l}Re^{1/2}N, \theta = \frac{T\text{-}T_\infty}{T_w\text{-}T_\infty}, \varphi = \frac{C - C_\infty}{C_w - C_\infty} \tag{7}$$

where, $Re = \frac{U_\infty L}{\upsilon}$.

By introducing Eq. (7) into Eqs. (1)–(5), the dimensionless PDEs can be obtained:

$$\frac{\partial U}{\partial X} + \frac{\partial V}{\partial Y} = 0 \tag{8}$$

$$U\frac{\partial U}{\partial X} + V\frac{\partial U}{\partial Y} = (1 + K)\frac{\partial^2 U}{\partial Y^2} - MU + K\frac{\partial N}{\partial Y} \tag{9}$$

$$U\frac{\partial N}{\partial X} + V\frac{\partial N}{\partial Y} = (1 + K/2)\frac{\partial^2 U}{\partial Y^2} - K\left(2N + \frac{\partial U}{\partial Y}\right) \tag{10}$$

$$U\frac{\partial \theta}{\partial X} + V\frac{\partial \theta}{\partial Y} = \frac{1}{Pr}\frac{\partial^2 \theta}{\partial Y^2} + (1 + K)Ec\left(\frac{\partial U}{\partial Y}\right)^2 + Df\frac{\partial^2 \varphi}{\partial Y^2} \tag{11}$$

$$U\frac{\partial \varphi}{\partial X} + V\frac{\partial \varphi}{\partial Y} = \frac{1}{Sc}\frac{\partial^2 \varphi}{\partial Y^2} + Sr\frac{\partial^2 \theta}{\partial Y^2} \tag{12}$$

in Eqs. (8)–(12), material parameter $K = \frac{\mu_r}{\mu_f}$, magnetic field parameter $M = \frac{\sigma B_0^2}{\rho_f c_p}$, Eckert number $Ec = \frac{U_\infty{}^2}{c_p(T_w\text{-}T_\infty)}$, Schmidt number $Sc = \frac{\nu}{D_m}$, Dufour coefficient $Df = \frac{D_m k_T}{c_s c_p \nu}\frac{(C_w\text{-}C_\infty)}{(T_w\text{-}T_\infty)}$, Soret coefficient $Sr = \frac{D_m k_T}{T_m \nu}\frac{(T_w\text{-}T_\infty)}{(C_w\text{-}C_\infty)}$.

Accordingly, the dimensionless boundary conditions are as follows:

$$Y = 0 : U = X + \delta\frac{\partial U}{\partial Y}, V \to 0, N = -\frac{1}{2}\frac{\partial U}{\partial Y}, \theta = 1, \varphi = 1 \tag{13}$$

$$Y \to \infty : U \to 0, N \to 0, \theta \to 0, \varphi \to 0$$

where, $\delta = A\sqrt{\frac{c}{\nu}}$.

The expressions of Nusselt number Nu_x and Sherwood number Sh_x are deduced as:

$$Nu_x = \frac{\text{-}x\frac{\partial T}{\partial y}}{T_w\text{-}T_\infty} + Df\frac{\text{-x}\frac{\partial C}{\partial y}}{\text{C}_w\text{-C}_\infty} = -\text{XRe}^{1/2}\frac{\partial \theta}{\partial \text{Y}} - DfXRe^{1/2}\frac{\partial \varphi}{\partial Y};\ Sh_x = \frac{\text{-}x\frac{\partial C}{\partial y}}{C_w\text{-}C_\infty} + Sr\frac{\text{-}x\frac{\partial T}{\partial y}}{T_w\text{-}T_\infty} = -XRe^{1/2}\frac{\partial \varphi}{\partial Y} - SrXRe^{1/2}\frac{\partial \theta}{\partial Y}. \tag{14}$$

Eq. (14) can be further rewritten as:

$$Re_x{}^{-1/2}Nu_x = -XRe_x{}^{-1/2}Re^{1/2}\left.\frac{\partial \theta}{\partial Y}\right|_{Y=0} - DfXRe_x{}^{-1/2}Re^{1/2}\left.\frac{\partial \varphi}{\partial Y}\right|_{Y=0} = -\left.\frac{\partial \theta}{\partial Y}\right|_{Y=0} - Df\left.\frac{\partial \varphi}{\partial Y}\right|_{Y=0} \tag{15}$$

$$Re_x{}^{-1/2}Sh_x = -XRe_x{}^{-1/2}Re^{1/2}\left.\frac{\partial \varphi}{\partial Y}\right|_{Y=0} - SrXRe_x{}^{-1/2}Re^{1/2}\left.\frac{\partial \theta}{\partial Y}\right|_{Y=0} = -\left.\frac{\partial \varphi}{\partial Y}\right|_{Y=0} - Sr\left.\frac{\partial \theta}{\partial Y}\right|_{Y=0}$$

3. Numerical simulations

3.1. Numerical method

It is popular to transform the original governing boundary layer PDEs into the higher ordinary ones through self-similar transformations. Then, numerical methods such as finite difference method or finite element method are adopted to solve. Different from the above treatment, the origin PDEs are only converted into the dimensionless ones rather than self-similar transformation. CSM via MM is adopted. It is convenient and flexible to solve the PDEs and to present the 2-D characteristics of the boundary layer.

Firstly, the semi-infinite region is transformed into an interval of $[X_1, X_2) \times [Y_1, Y_2]$, a semi-open interval in X direction and a closed

Table 1
Absolute errors corresponding to various grids.

$Nx \times Ny$	ε_U	ε_V	ε_θ
5 × 10	2.915×10^{-4}	1.9635×10^{-3}	1.3462×10^{-3}
5 × 20	4.5812×10^{-11}	4.2239×10^{-10}	2.9400×10^{-7}
5 × 25	1.8207×10^{-13}	1.3497×10^{-12}	6.1652×10^{-9}
5 × 30	2.2611×10^{-13}	3.5658×10^{-12}	1.3298×10^{-10}
5 × 32	3.7821×10^{-13}	5.2943×10^{-12}	2.3675×10^{-11}
5 × 34	1.8900×10^{-13}	4.5159×10^{-12}	2.0409×10^{-12}
5 × 35	2.3164×10^{-13}	6.6487×10^{-12}	1.3811×10^{-12}
8 × 35	2.0794×10^{-13}	7.5863×10^{-12}	1.3816×10^{-12}
10 × 35	2.3038×10^{-12}	7.3529×10^{-12}	1.3812×10^{-12}

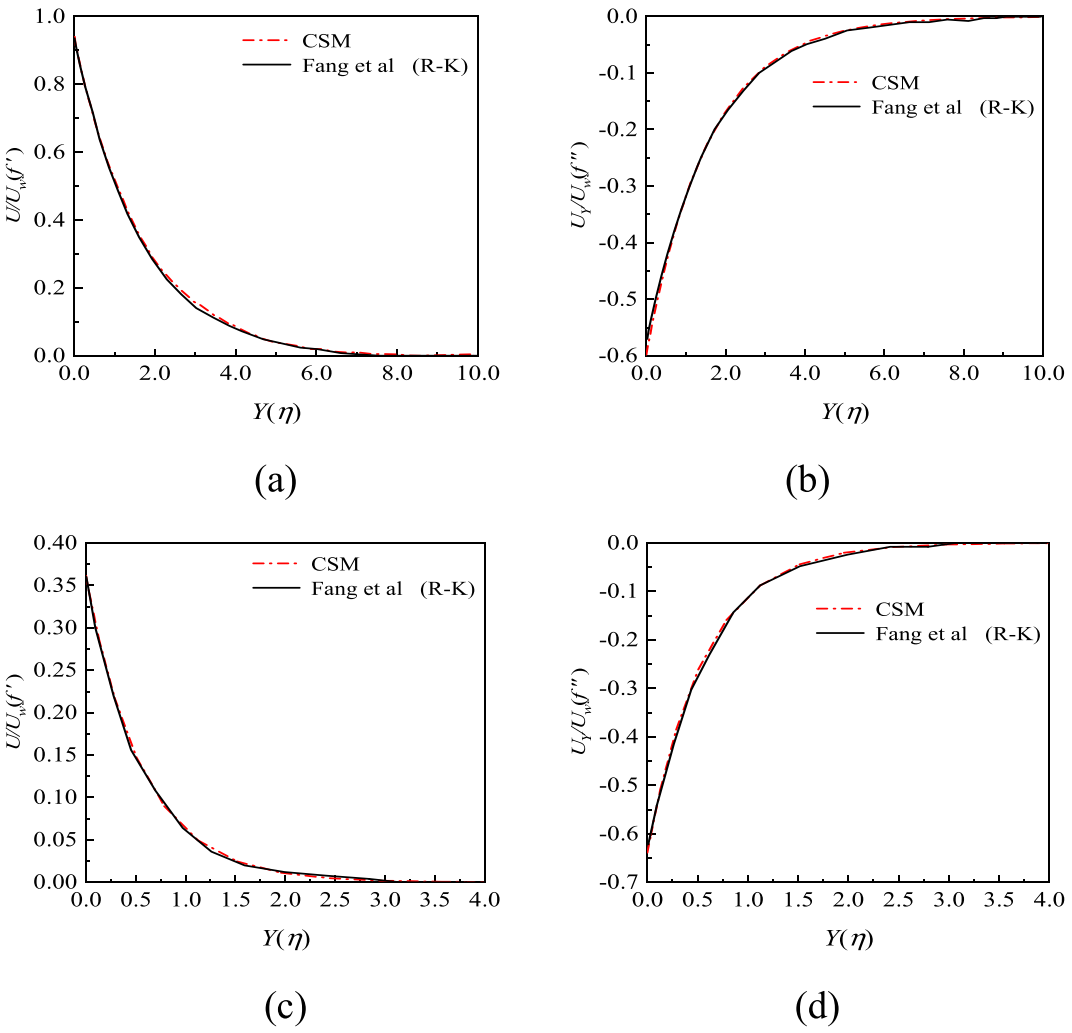

Fig. 2. Comparisons of the dimensionless U and $\partial U/\partial Y$ curves against $Y(\eta)$ with $\delta = 1$ and $M = 1$ for s = -1 from (a) to (b) and $s = 1$ from (c) to (d).

interval in the Y direction. Thereafter, Chebyshev-Gauss-Radau (CGR) and Chebyshev-Gauss-lobatto (CGL) collocation points in X direction and Y direction are selected for discretization, respectively. The physical model is transformed from physical space into spectral space [-1, 1) ×[-1, 1] using the following equations [55]:

$$s_{x,i} = cos\frac{2\pi i}{2N_x + 1}, i = 0, 1, \cdots N_x \tag{16}$$

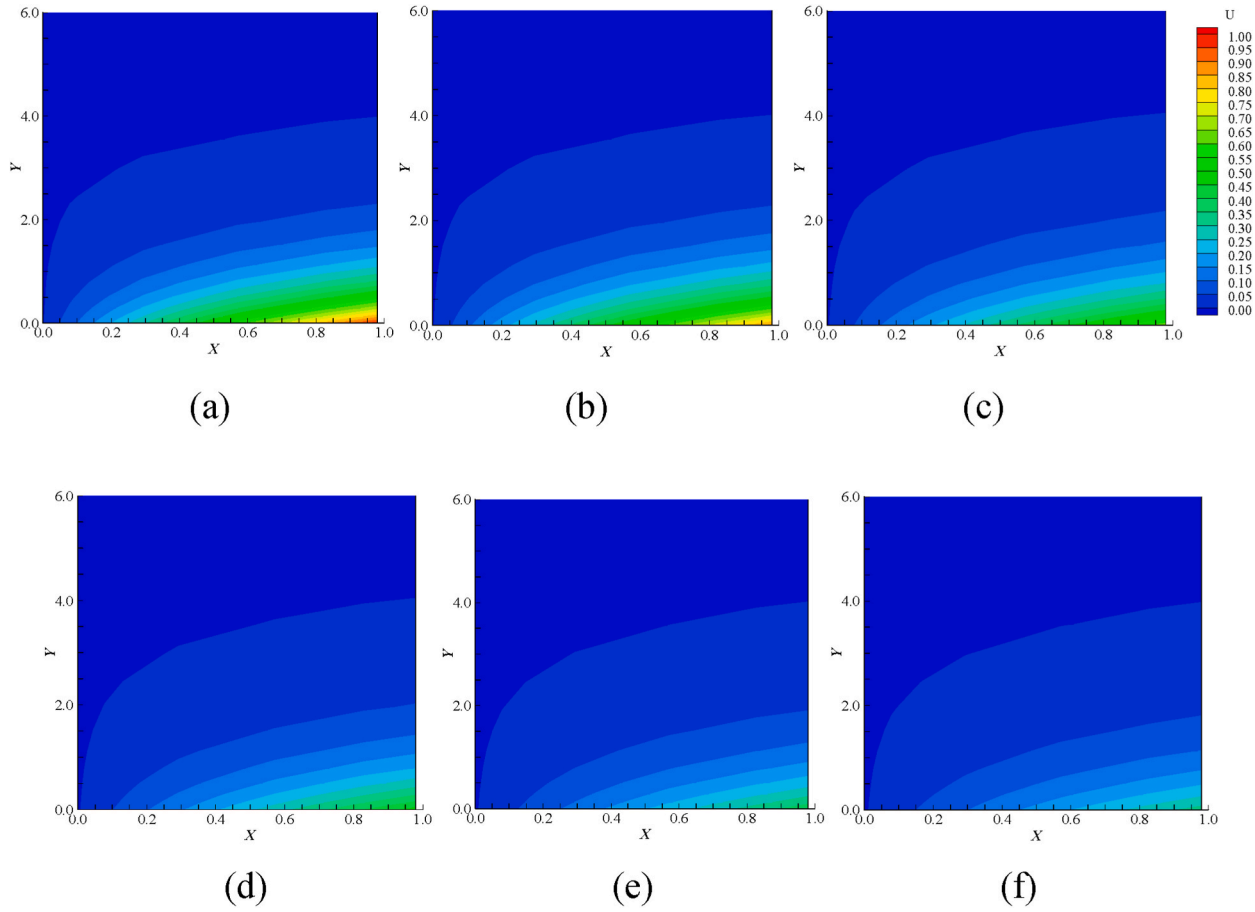

Fig. 3. Distributions of dimensionless velocity component U with first-order slip parameter δ ((a) $\delta = 0.0$; (b) $\delta = 0.1$; (c) $\delta = 0.5$; (d) $\delta = 1.0$; (e) $\delta = 1.5$; (f) $\delta = 2.0$).

$$s_{y,j} = cos\frac{\pi j}{N_y}, j = 0, 1, \cdots N_y$$

The dimensionless variables can be approximated by the Lagrange interpolation polynomial. The convergence criterion is $\left|\varphi_{ij}^{n+1} - \varphi_{ij}^{n}\right| < \varepsilon$, φ represents U, V, θ and φ. n represents the number of iterations. In the marching process, the most important steps are the solving of matrix equations. The matrix equations are solved by two-step direct solver. To save space, One can refer to our previously published paper [56,57] for more details for the treatment of semi-infinite domain, discretization and convergence settings.

3.2. Verifications

Before analysis of flow, heat and mass transfer of MHD MF boundary layer, the effectiveness and accuracy of CSM for solving boundary layer problems are verified with those in Refs. [58,59]. When $Pr = 1, K = 0, M = 0, Ec = 0, Df = 0, \delta = 0$, exact solutions are gained as:

$$U = Xe^{-Y}, V = -1 + e^{-Y}, \theta = \frac{e}{e-1}\left(1 - e^{-e^{-Y}}\right)$$

Grid independent evaluation of CSM is performed. The grid sizes are tested from 5×10 to 10×35. Table 1 gives the absolute accuracies of velocity and temperature with various grids. It can be seen from Table 1 that the absolute accuracies of grids 5×30 by CSM can reach the order of 10^{-12}, which indicates the accuracy and efficiency of CSM for boundary layer problem.

Next, MHD boundary flow with slip condition is tested with Fang [59]. After appropriate simplification, the model established in this work is in consistent with that in Ref. [59]. The comparisons between SCM and R–K method [59] are shown in Fig. 2(a–d). The velocity and velocity gradient curves against $Y(\eta)$ axis by CSM are almost coincide with those of R–K method. It further confirms the feasibility and highly accuracy of the mathematical model and the numerical method adopted here for the boundary layer problem of MHD micropolar nanofluid.

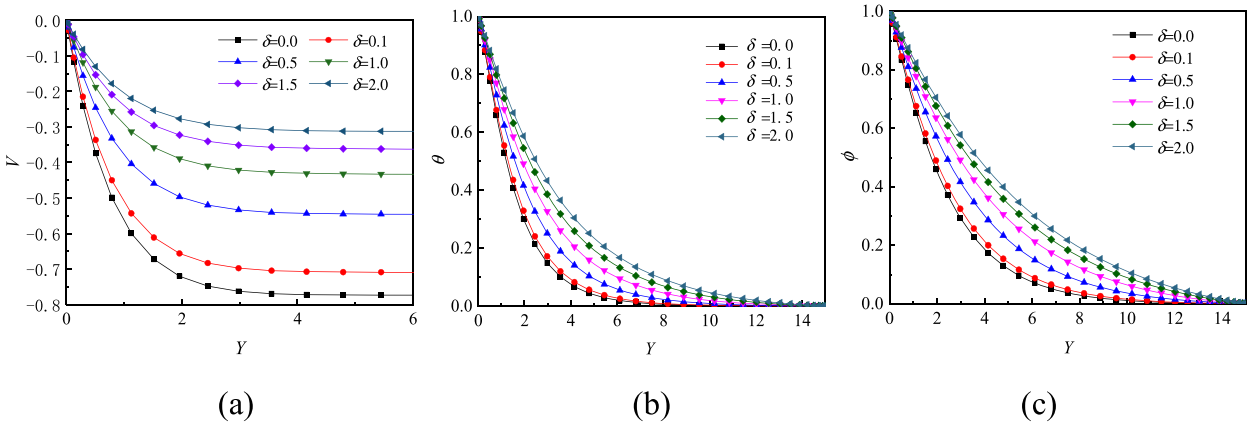

Fig. 4. Dimensionless velocity component V, temperature θ and concentration φ curves against Y with first-order slip parameter δ ((a) V; (b) θ ; (c) φ).

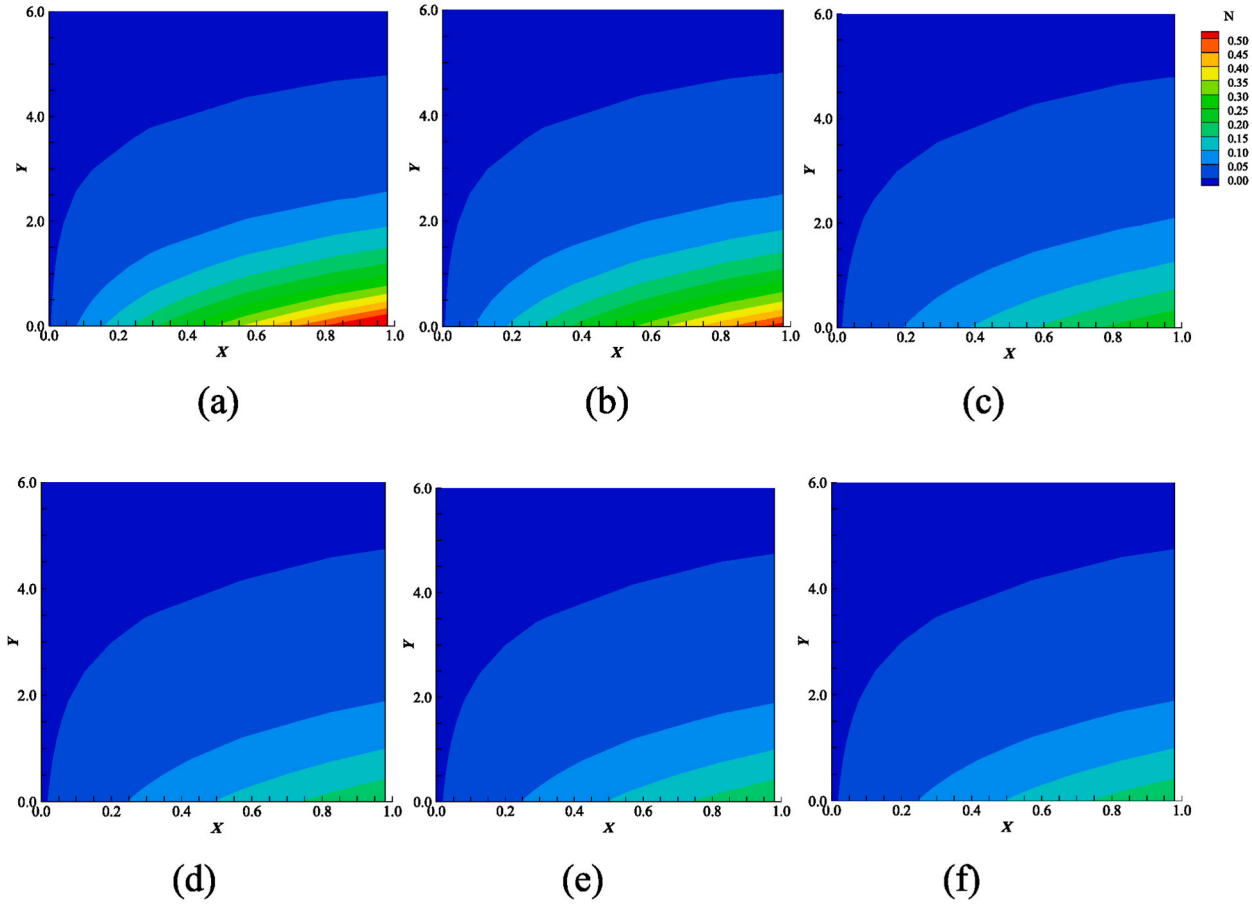

Fig. 5. Distributions of dimensionless angular velocity N with first-order slip parameter δ ((a) $\delta = 0.0$; (b) $\delta = 0.1$; (c) $\delta = 0.5$; (d) $\delta = 1.0$; (e) $\delta = 1.5$; (f) $\delta = 2.0$).

4. Results analysis and discussion

In this section, flow, heat and mass transfer of MHD micropolar nanofluid in the boundary layer of a stretching plate by the action of first-order slip parameter δ, viscous dissipation coefficient Ec, material parameter K, magnetic field parameter M, Dufour coefficient Df and Soret coefficient Sr are discussed and analyzed. Heat and mass transfer rates of MHD micropolar nanofluid are revealed through

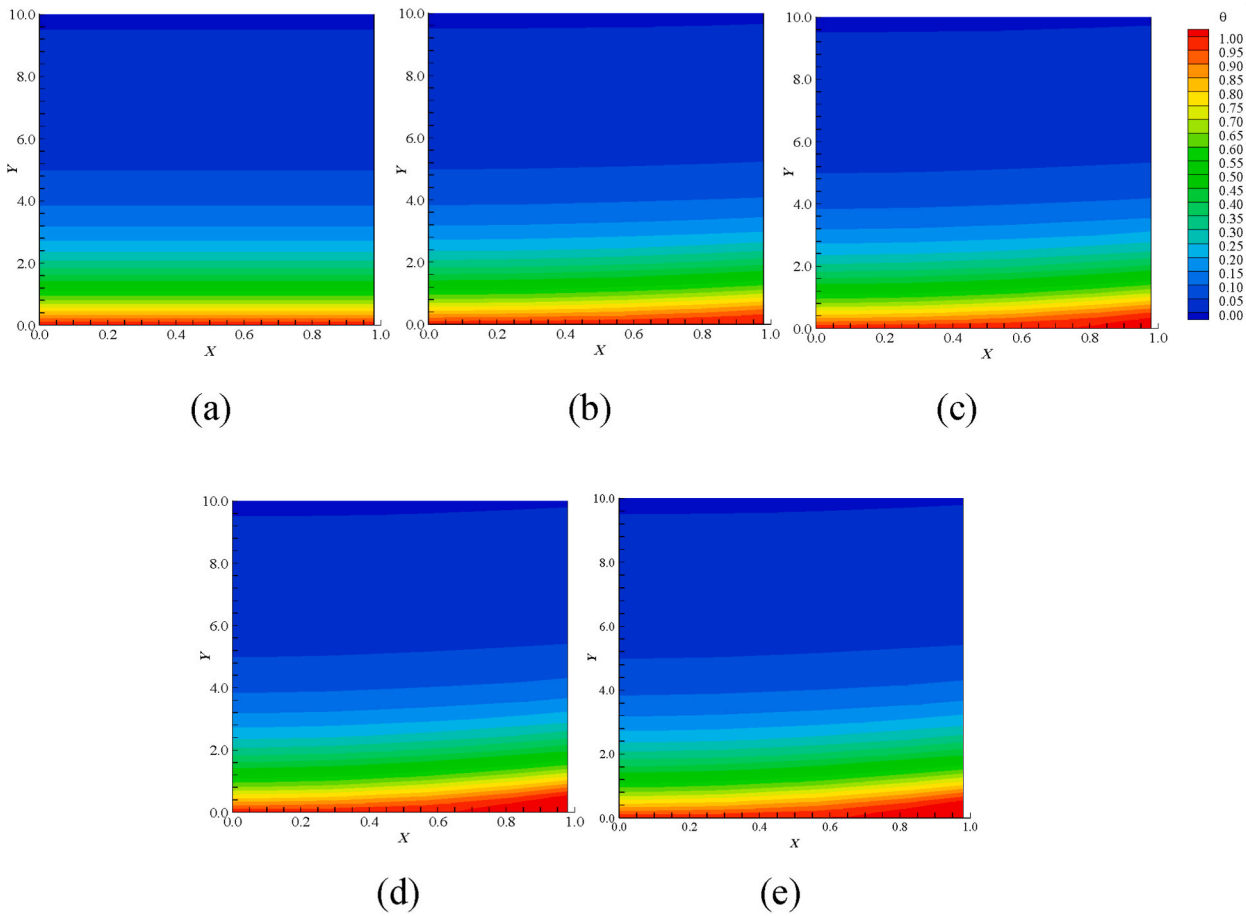

Fig. 6. Distribution of dimensionless temperature θ with Ec ((a) $Ec = 0.0$; (b) $Ec = 0.5$; (c) $Ec = 1.0$; (d) $Ec = 1.5$; (e) $Ec = 2.0$).

local Nu and Sh curves on the wall. The relevant parameters are defined as: $Pr = 1$, $K = 0.5$, $M = 1$, $Sc = 0.5$, $Ec = 0.5$, $Df = 0.1$, $Sr = 0.1$, $\delta = 0.1$.

4.1. *Influences of first-order slip boundary condition*

Velocity slip is a finite velocity boundary condition between a fluid and a surface. When micropolar nanoparticles are added to the base fluid, local velocity slip may occur due to the high shear force between the fluid and the wall, thus the slip condition is no longer negligible at the nano or micron scale. Figs. 3 and 4 display the velocity component U distribution and V curve with the effect of the first-order slip parameter δ in the boundary layer. As can be seen from Fig. 3(a–f), with the increasing , U at the wall decreases obviously, confirming that there is an evident slip movement between the fluid and the stretching plate. The velocity distribution inside the boundary layer is influenced. Correspondingly, less fluid is driven from the main stream to the boundary layer. As a consequence, the absolute value of V decreases with the increase of δ (as shown in Fig. 4(a)). Fig. 5(a–f) depicts the effect of δ on the distribution of the angular velocity N in the boundary layer. With the rise of δ, N declines clearly in the vicinity of the surface. From the physical point of view, the above phenomenon is due to the decrease of the linear velocity of the fluid, which in turn affects N. Fig. 4(b) and (c) exhibit the influence of δ on the dimensionless temperature θ and the dimensionless concentration φ curves in the boundary layer. Since thermal convection dominates heat transfer, the velocity slip effect can further influence heat and mass transfer. The increase of δ immediately results in the continuous increase of θ from Fig. 4(b). The similar trend of φ curve can be found, while its variational amplitude is larger than that of θ (Fig. 4(c)). The temperature boundary layer and concentration boundary layer both become thicker accordingly. These results also reflect that the velocity field in the boundary layer plays a vital role in affecting the transport process of the system. In addition, it is worth noting that there is a coupling interaction between the temperature and concentration transport, the actual temperature and concentration in the boundary layer is underestimated as the slip boundary condition is not taken into account. Based on this, the classical no-slip condition is no longer suitable for the study of MF flow. The decrements of linear velocity components U and V at the right corner of the plate, can reach by about 66.96% and 59.56% respectively, in the consideration of first-order slip velocity model compared with the non-slip one. Further, the angular velocity N reduces by about 73.21%. Both θ and φ increase by about 46.15% and 46.25% with the same parameters.

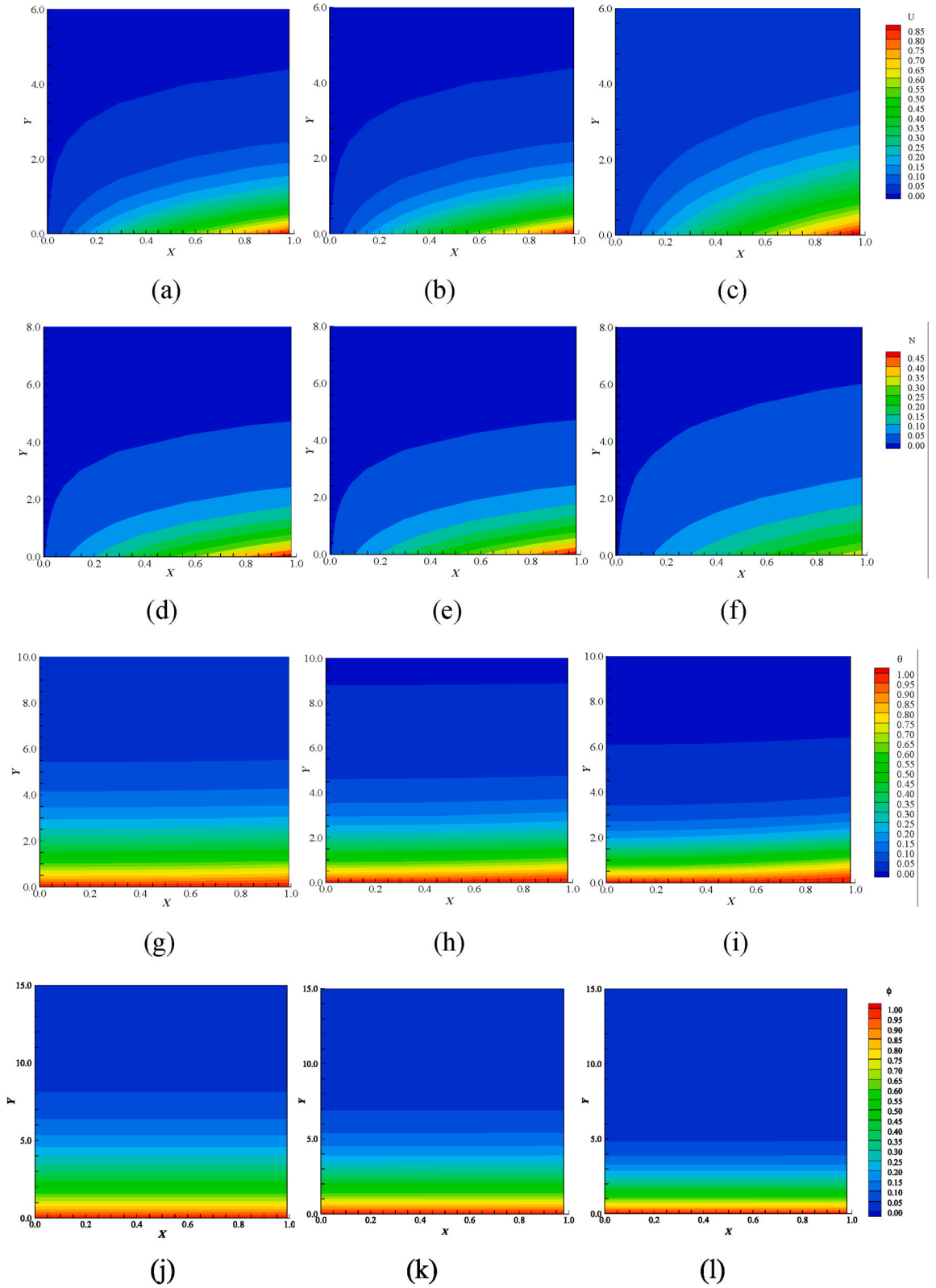

Fig. 7. Distributions of dimensionless angle velocity N, temperature θ and concentration φ with material parameter $K = 0.0, 1.0, 5.0$ from left to right (U from (a) to (c); N from (d) to (f); θ from (g) to (i); φ from (j) to (l)).

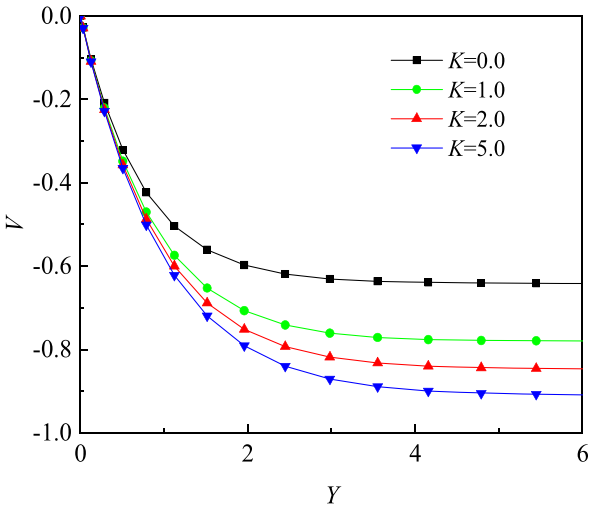

Fig. 8. Variation curves of dimensionless velocity component V with material parameter K.

4.2. Influences of viscous dissipation

Eckert number, which is related to viscous thermal effect, reflects heat dissipation converted from mechanical energy to thermal energy through internal friction. The enthalpy difference can be associated with the kinetic energy successfully by this critical number. Fig. 6(a–e) visualizes the effect of Ec on θ distribution. As Ec increases, dimensionless temperature θ at the surface increases gradually, especially in the region far from the origin, where it is even higher than the wall temperature. Due to viscous dissipation, the dimensionless temperature at the wall surface can reach up to 1.05 when $Ec = 2.0$. The physical reason is the internal energy converted from the kinetic energy by the viscous stress of MF. As a consequence, the temperature of micropolar nanofluid rises by mechanical energy dissipated into thermal energy.

4.3. Influence of material parameters

Material parameter K is the ratio of vortex viscosity μ_r to dynamic viscosity μ_f. That is, the larger the material parameter K, the smaller the dynamic viscosity. Figs. 7 and 8 portray the influence of material parameter K on the boundary layer. It is noticed from Fig. 7(a)–(c) that nearly no variation of U can be seen for small value of K; as K rises to the value of 1.0, U escalates and the boundary layer thickens with increasing K. Material parameter K causes an increment of approximately 60% in the thickness of the linear velocity boundary. The absolute value of velocity V increases gradually as seen in Fig. 8. Greater K promotes the MF flow obviously. This is due to the descent of the dynamic viscosity, which elevate the overall magnitude of flow momentum. Therefore, the velocity of the fluid increases with the rise of K. Fig. 7(d)–(f) depict the angular velocity distribution N with K. According to the definition of K, an increase in K means a lift in the vortex viscosity μ_r. Therefore, the variational trend of the N is opposite to those of U and V, and the thickness of N boundary layer becomes broaden. This is because the increase of μ_r strengthens the friction between the particles and the adjacent fluid, and inhibits the rotation of micropolar particles. Compared with that of Newtonian fluid, the maximum angle velocity of micropolar nanofluid can be sufficiently reduced by about 43.33% on the boundary surface, when $K = 5.0$. Fig. 7 (g)–(i) and (j) to (l) present the distributions of the temperature θ and the concentration φ with the influence of K. Since fluid flow plays a dominant role in the process of affecting the transport of the boundary layer, as K inhibits flow of MF, further affects heat and mass transfer, an increase in K decays the value of θ and the thickness of thermal boundary layer. Similar variational trend of φ with K can be observed to those of θ. The decrement of concentration boundary layer thickness by about 37.50% is reached when $K = 5.0$.

4.4. Influences of magnetic field

Distributions of U, N and θ with effect of magnetic field parameter M are illustrated in Fig. 9(a–i). It is observed that from Fig. 9 (a)–(c) with the increase of M, U decreases gradually and the boundary layer thickness becomes thinner. Lorentz force by applying magnetic field tends to hinder fluid movement. With the increase of M, the stronger the magnetic field intensity, the more obvious the inhibition effect and the slower the fluid velocity, which is confirmed by the decrease of the velocity distribution of the boundary layer. Magnetic field has great influence on the thickness of the velocity boundary layer thickness. Discrepancies of the average velocities are about 64.29% and 8.5% with and without the magnetic field ($M = 5$). Different from the distribution of U, the opposite effect of M towards N is gained, while the boundary layer thickness is almost unchanged (from Fig. 9(d)–(f)). With the influence of magnetic field ($M = 5$), the angular velocity at the right corner in the boundary increases as highly as 118%. The effect of M on θ is furnished in Fig. 9. (from (g)–(i)). With the increase of M, θ increases and the boundary layer thickness increases. As M increases, the additional work done by the fluid against the counterforce of the transverse magnetic field is accumulated, resulting in the increase of heat. Therefore, the

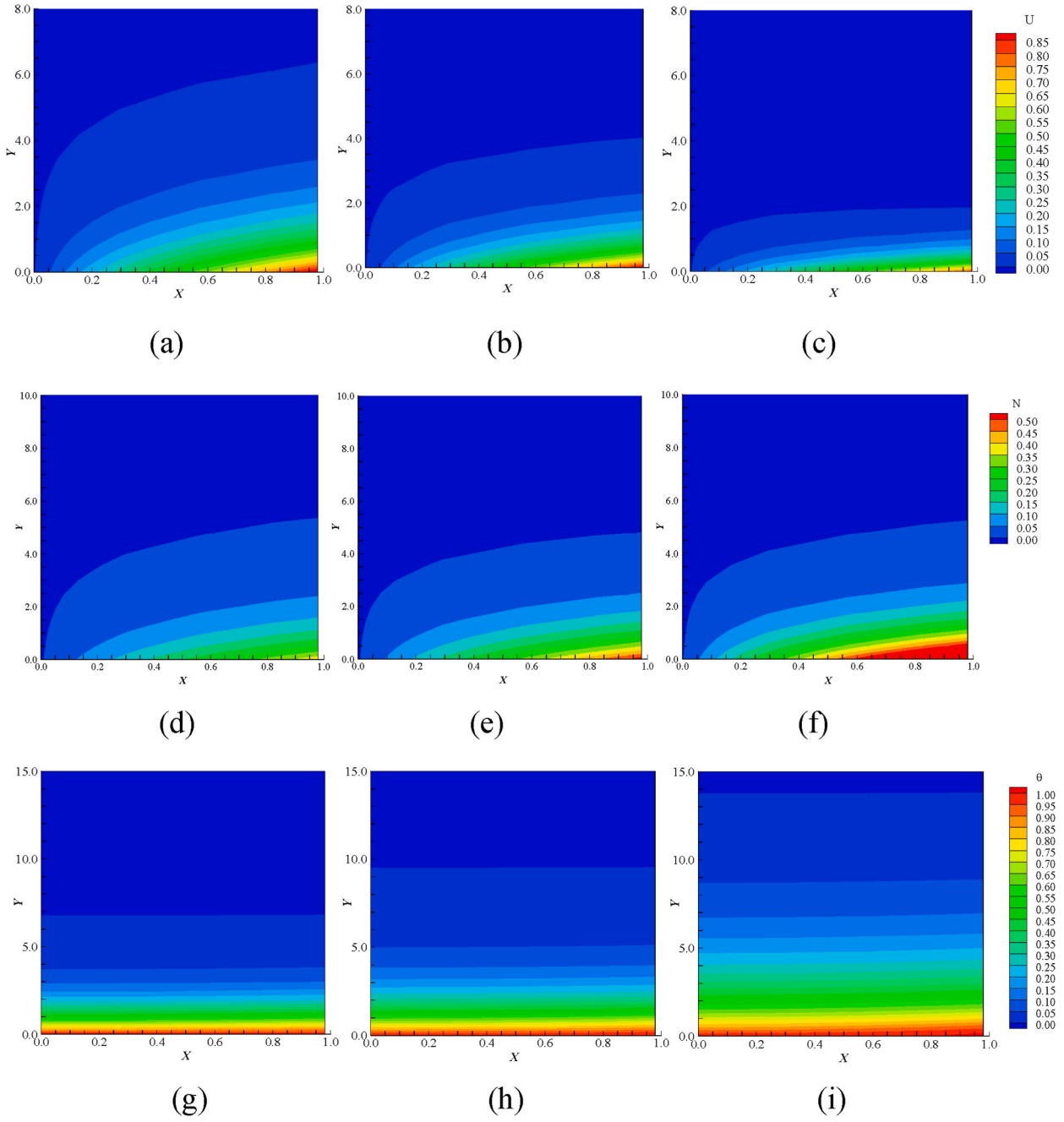

Fig. 9. Distribution of U, N and θ with various magnetic parameter $M = 0.0, 1.0, 5.0$ (U from (a) to (c); N from (d) to (f); θ from (g) to (i)).

dimensionless temperature θ goes up. φ profile presents similar variation trend of θ which not presented for saving space.

4.5. Influences of cross diffusion

Dufour effect refers to heat transfer caused by concentration gradient. The concentration gradient promotes thermal diffusion, which enhances Dufour effect and leads to the increase of temperature. On the contrary, Soret effect refers to mass transfer caused by temperature gradient. Due to the extremely highly coupling relationship between Dufour effect and Soret effect, Soret effect can't depart from Dufour effect. Fig. 10(a and b) visualizes the influence of Df on temperature (a) and Sr on concentration (b) profiles, respectively. It can be seen from Fig. 10(a) that θ profile within the boundary layer becomes more uniform, and the value of the average temperature is observed to rise by about 79.73% with Dufour effect. With the increase of Sr, φ distribution increases for additional

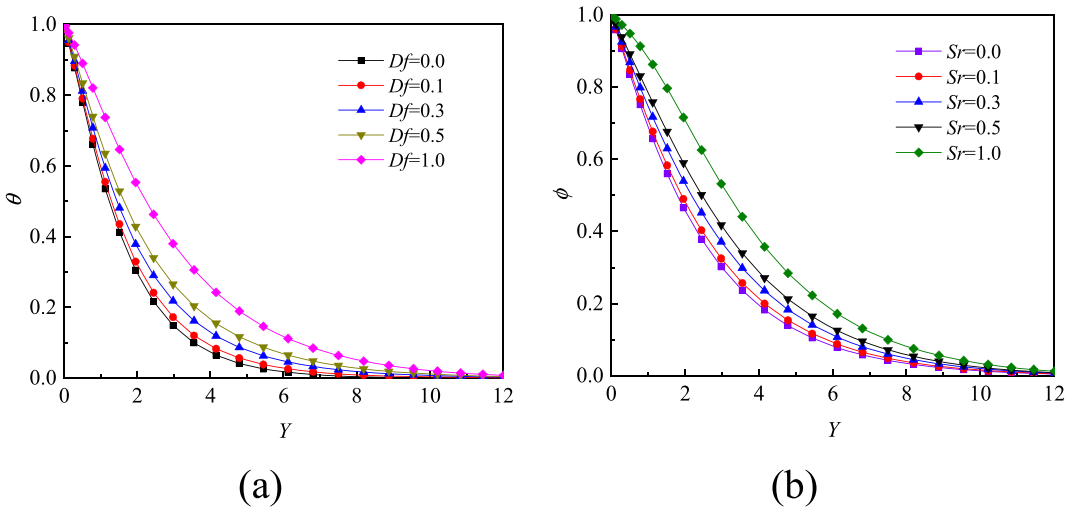

Fig. 10. Variation curves of dimensionless temperature θ with *Df* and of dimensionless concentration φ with *Sr* ((a) θ curve; (b) φ curve).

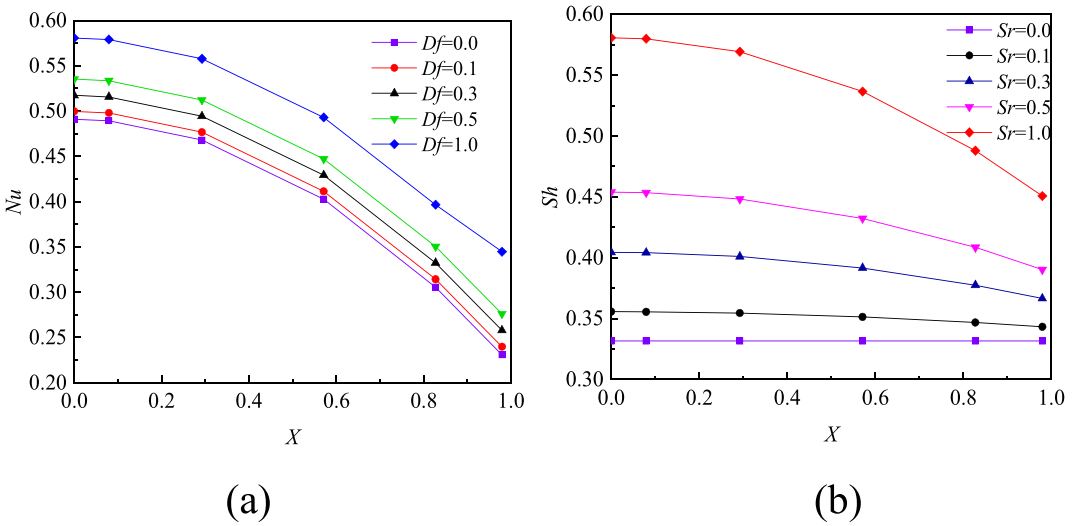

Fig. 11. Variation curves of *Nu* with *Df* and of *Sh* with *Sr* ((a) *Nu* curve; (b) *Sh* curve).

diffusion caused by temperature gradient (Fig. 10(b)). Fig. 11(a and b) shows the variation local *Nu* curve and local *Sh* curve with *Df* and *Sr*, respectively. Proportional growth in *Nu* is found along *X* coordinate along the plate surface with increasing *Df* due to the promotion of Dufour effect on heat transfer on the wall. Compared with the influence of Dufour effect on temperature, the augment of *Sh* by a factor of about 38.15% as can be found with Soret effect in Fig. 11(b).

5. Conclusions

In this work, numerical simulations of cross diffusive boundary layer flow of MHD micropolar nanofluid on a lubricated surface are carried out successfully using CSM. The process of laminar flow, heat and mass transfer in the boundary layer with the action of a steady magnetic field is analyzed. The effects of first order slip parameter δ, material parameter *K*, magnetic field parameter *M*, viscous dissipation *Ec*, Dufour effect parameter *Df* and Soret effect parameter *Sr* are examined. The significant consequences are drawn as follows:

1) The slip effect can be enhanced with the help of first-order slip parameters δ on the stretching plate, further the velocity, temperature and concentration reduced accordingly. The angular velocity reduces by about 73.21%. Both the dimensionless temperature and concentration increase by about 46.15% and 46.25% with the same parameters.

2) As Ec increases, more mechanic energy converts into thermal energy; which leads to temperature elevation. The dimensionless temperature at the wall surface can reach up to 1.05 when $Ec = 2.0$.
3) Linear velocity of MF is speeded up; while angular velocity is reduced with material parameter K. The maximum angle velocity can be reduced sufficiently by about 43.33% on the boundary surface.
4) The increase of M inhibits fluid flow and results in the boost in temperature. Discrepancies of the average velocities are about 64.29% and 8.5%; besides, the angular velocity at the right corner in the boundary increases as highly as 118% with and without the magnetic field.
5) The cross-diffusion promotes heat and mass transfer and enhances temperature and concentration of MF. Temperature θ profile within the boundary layer becomes more uniform, and the value of average temperature is observed to rise by about 79.73% with Dufour effect. The augment of Sh by a factor of about 38.15% as can be found with Soret effect.

The basic study on laminar flow, heat and mass transfer of MHD MFs in boundary layer has been performed in this paper. In the future, we will continue to conduct further research on this subject, and carry out the instability analysis of MHD MF flow with the action of thermomagnetic effect, so as to discover the vital factors in the fluid flow control.

Data availability statement

Data will be made available on request.

CRediT authorship contribution statement

Xiyan Tian: Writing – original draft, Funding acquisition, Conceptualization. **Bingbing Yang:** Software. **Xin Na:** Formal analysis. **Liankang Ba:** Validation. **Yi Yuan:** Funding acquisition, Data curation.

Declaration of competing interest

The authors declare that they have no known competing financial interests or personal relationships that could have appeared to influence the work reported in this paper.

Acknowledgements

This work was supported by Natural Science Foundation of Liaoning Province of China (2021-MS-084) and the Natural Science Foundation of China (NSFC) with granted contracts (52274407).

Nomenclature

A	first order slip coefficient
B_0	magnetic field strength
c	a constant
c_p	specific heat at constant pressure
C	solutal concentration
Df	Dufour diffusivity
D_m	mass diffusion
Ec	Eckert number
j	micro-inertial density
K	material parameter
M	magnetic field parameter
n	number of iterations
N	Angular velocity
Nu_x	Nusselt number
Pr	Prandtl number
Re	Reynolds number
Sc	Schmidt number
Sh_x	Sherwood number
Sr	Soret coefficient
T	temperature
x, y	Cartesian axes
X, Y	Dimensionless Cartesian axes
u, v	velocity components in x and y directions
U, V	dimensionless velocity components in X and Y directions

Greek symbols

γ	spin-gradient viscosity
μ_f	dynamic viscosity
μ_r	vortex viscosity
ω	Dimensionless angular velocity
Δ	first-order slip coefficient

subscripts

W	wall
∞	Ambient conditions

References

[1] A.C. Eringen, Theory of micropolar fluids, Indiana Univ. Math. J. 16 (1) (1967) 1–18, https://doi.org/10.1512/iumj.1967.16.16001.
[2] D.B. Holmes, J.R. Vermeulen, Velocity profiles in ducts with rectangular cross sections, Chem. Eng. Sci. 23 (7) (1968) 717–722, https://doi.org/10.1016/0009-250, 9(68)85006-85007.
[3] J. Chen, C. Liang, J.D. Lee, Theory and simulation of micropolar fluid dynamics, Proc. Inst. Mech. Eng. C. J. Mech. Eng. Sci. 224 (1) (2011) 31–39, https://doi.org/10.1177/1740349911400132.
[4] H.A. Hogan, M. Henriksen, An evaluation of a micropolar model for blood flow through an idealized stenosis, J. Biomech. 22 (3) (1989) 211–218, https://doi.org/10.1016/0021-9290(89)90089-4.
[5] P. Valipour, S.E. Ghasemi, M. Vatani, Theoretical investigation of micropolar fluid flow between two porous disks, J. Cent. South Univ. 22 (2015) 2825–2832, https://doi.org/10.1007/s11771-015-2814-1.
[6] N.T. Eldabe, M.Y. Abou-Zeid, The wall properties effect on peristaltic transport of micropolar non-Newtonian fluid with heat and mass transfer, Math. Probl Eng. 2010 (2010) 898062, https://doi.org/10.1155/2010/898062.
[7] N.T.M. Eldabe, M.A. Hassan, M.Y. Abou-Zeid, Wall properties effect on the peristaltic motion of a coupled stress fluid with heat and mass tran-sfer through a porousmedium, J. Eng. Mech. 142 (3) (2015) 04015102, https://doi.org/10.1061/(ASCE)EM.1943-7889.0001029.
[8] W. Ibrahim, MHD boundary layer flow and heat transfer of micropolar fluid past a stretching sheet with second order slip, J. Braz. Soc. Mech. Sci. 39 (2017) 791–799, https://doi.org/10.1007/540430-016-0621-8.
[9] F. Mabood, A. Shafiq, T. Hayat, S. Abelman, Radiation effects on stagnation point flow with melting heat transfer and second order slip, Results, Phys. Met. 7 (2017) 31–42, https://doi.org/10.1016/j.rinp.2016.11.051.
[10] N. Eldabe, G. Saddeck, A.F. El-sayed, Heat transfer of MHD non-Newtonian Casson fluid flow between two rotating cylinders, Mech. Eng. 5 (2001) 230–250. https://api.semanticscholar.org/CorpusID:119037337.
[11] Y.S. Daniel, S.K. Daniel, Effects of buoyancy and thermal radiation on MHD flow over a stretching porous sheet using homotopy analysis method, Alex, Eng. J. 54 (3) (2015) 705–712, https://doi.org/10.1016/j.aej.2015.03.029.
[12] Y.S. Daniel, Steady MHD laminar flows and heat transfer adjacent to porous stretching sheets using HAM, Am. J. Heat Mass Transf 2 (2015) 146–159, https://doi.org/10.7726/ajhmt.2015.1010.
[13] Y.S. Daniel, Z.A. Aziz, Z. Ismail, F. Salah, Entropy analysis in electrical magnetohydrodynamic (MHD) flow of nanofluid with effects of thermal radiation, viscous dissipation, and chemical reaction, Theor. App. Mech. Lett. 7 (4) (2017) 235–242, https://doi.org/10.1016/j.taml.2017.06.003.
[14] Y.S. Daniel, Z.A. Aziz, Z. Ismail, F. Salah, Double stratification effects on unsteady electrical MHD mixed convection flow of nanofluid with viscous dissipation and Joule heating, J. Appl. Res. Technol. 15 (2017) 464–476, https://doi.org/10.1016/j.jart.2017.05.007.
[15] Y.S. Daniel, Z.A. Aziz, Z. Ismail, F. Salah, Impact of thermal radiation on electrical MHD flow of nanofluid over nonlinear stretching sheet with variable thickness, Alex. Eng. J. 57 (2017) 2187–2197, https://doi.org/10.1016/j.aej.2017.07.007.
[16] S.Y. Daniel, A.Z. Aziz, Z. Ismail, F. Salah, Thermal stratification effects on MHD radiative flow of nanofluid over nonlinear stretching sheet with variable thickness, J. Comput. Des. Eng. 5 (2018) 232–242, https://doi.org/10.1016/j.jcde.2017.09.001.
[17] Y.S. Daniel, Z.A. Aziz, Z. Ismail, F. Salah, Numerical study of Entropy analysis for electrical unsteady natural magnetohydrodynamic flow of nanofluid and heat transfer, Chin, J. Phys. 55 (2017) 1821–1848, https://doi.org/10.1016/j.cjph.2017.08.00.
[18] Y.S. Daniel, Z.A. Aziz, Z. Ismail, F. Salah, Thermal radiation on unsteady electrical MHD flow of nanofluid over stretching sheet with chemical reaction, J. King Saud Univ. Sci. 31 (2019) 804–812, https://doi.org/10.1016/j.jksus.2017.10.002.
[19] Y.S. Daniel, Z.A. Aziz, Z. Ismail, F. Salah, Entropy analysis of unsteady magnetohydrodynamic nanofluid over stretching sheet with electric field, Int. J. Multiscale Comput. Eng. 15 (2017) 545–565, https://doi.org/10.1615/IntJMultCompEng.2017021952.
[20] S.D. Yahaya, U. Aliyu, H. Umaru, Stagnation point flow with thermal and magnetic field over a stretching sheet, World Sci.J. 2 (2017) 196–199.
[21] Y.S. Daniel, Z.A. Aziz, Z. Ismail, F. Salah, Hydromagnetic slip flow of nanofluid with thermal stratification and convective heating, Aust. J. Mech. Eng. 18 (2018) 147–155, https://doi.org/10.1080/14484846.2018.1432330.
[22] Y.S. Daniel, Z.A. Aziz, Z. Ismail, A. Bahar, F. Salah, Stratified electromagnetohydrodynamic flow of nanofluid supporting convective role, Kor. J. Chem. Eng. 36 (7) (2019) 1021–1032, https://doi.org/10.1007/s11814-019-0247-5.
[23] N. Eldabe, D. Mostapha, Hall current and Joule heating effects on peristaltic flow of a Sisko fluid with mild stenosis through a porous medium in a tapered artery with slip and convection boundary conditions, Sains Malays. 49 (5) (2020) 1175–1190, https://doi.org/10.17576/jsm-2020-4905-23.
[24] N. Eldabe, G. Saddeck, A.F. El-sayed, Heat transfer of MHD non-Newtonian Casson fluid flow between two rotating cylinders, Mech. Eng. 5 (2001) 230–250. https://api.semanticscholar.org/CorpusID:119037337.
[25] N.T. Eldabe, G.M. Moatimid, H.S. Ali, Magnetohydrodynamic flow of non-Newtonian Visco-elastic fluid through a porous medium near an accelerated plate, Can. J. Phys. 81 (11) (2003) 1249–1269, https://doi.org/10.1139/p03-092.
[26] Y.S. Daniel, A. Usman, U. Haruna, Effect of electric field flow on nanofluid over stretchable surface, Sci. World J. 1 (2017) 186–190.
[27] H.M. Shawky, N.T.M. Eldabe, K.A. Kamel, E.A. Abd-Aziz, MHD flow with heat and mass transfer of Williamson nanofluid over stretching sheet through porous medium, Microsyst. Technol. 25 (2019) 1155–1169, https://doi.org/10.1007/s00542-018-4081-1.
[28] N. Eldabe, M.A. Abouzeid, D. Roshdy, Y.M. Mohamed, M. Ouaf, Impacts of chemical reaction and electric field with Cattaneo christov theories on peristaltic transport of a hyperbolic micropolar nano fluid, Egypt, J. Chem. 66 (2023) 63–85, https://doi.org/10.21608/ejchem.2022.165317.7033.
[29] S.O. Salawu, R.A. Oderinu, A.D. Ohaegbue, Thermal runaway and thermodynamic second law of a reactive couple stress hydromagnetic fluid with variable properties and Navier slips, Sci. Afr. 7 (2020) e00261, https://doi.org/10.1016/j.sciaf.2019.e00261.
[30] K.A. Kumar, V. Sugunamma, N. Sandeep, Impact of non-linear radiation on MHD non-aligned stagnation point flow of micropolar fluid over a convective surface, Int. J. Appl. Mech. 43 (4) (2018) 327–345, https://doi.org/10.1515/jnet-2018-0022.

[31] F. Mabood, W.A. Khan, Analytical study for unsteady nanofluid MHD Flow impinging on heated stretching sheet, J. Mol. Liq. 219 (2016) 216–223, https://doi.org/10.1016/j.mollig.2016.02.071.
[32] P.V.S. Narayana, B. Venkateswarlu, S. Venkataramana, Effects of hall current and radiation absorption on MHD micropolar fluid in a rotating system, Ain Shams Eng. J. 4 (4) (2013) 843–854, https://doi.org/10.1016/j.asej.2013.02.002.
[33] M. Waqas, M. Farooq, M.I. Khan, A. Alsaedi, T. Hayat, T. Yasmeen, Magnetohydrodynamic (MHD) mixed convection flow of micropolar liquid due to nonlinear stretched sheet with convective condition, Int. J. Heat Mass Tran. 102 (2016) 766–772, https://doi.org/10.1016/j.ijheatmasstransfer.2016.05.142.
[34] L. Dianchen, M. Ramzan, A. Shafiq, C.J. Dong, F. Umer, A numerical treatment of MHD radiative flow of micropolar nanofluid with homogenous heterogeneous reactions past a nonlinear stretched surface, Sci. Rep. 8 (1) (2018) 12431, https://doi.org/10.1038/541598-018-30965-x.
[35] G.V.R. Reddy, Y.H. Krishna, Soret and Dufour effects on MHD micropolar fluid flow over a linearly stretching sheet, through a non-Darcy porous medium, Int. J. Appl. Mech. 23 (2) (2018) 485–502, https://doi.org/10.2478/ijame-2018-0028.
[36] E.O. Fatunmbi, A. Adeniyan, Heat and mass transfer in MHD micropolar fluid flow over a stretching sheet with velocity and thermal slip conditions, O. J. F. D. 8 (2) (2018) 195–216, https://doi.org/10.4236/ojfd.2018.82014.
[37] M. Rizwan, M. Hassan, M.I. Asjad, E.M. Tag-ElDin, Flow characteristics of heat and mass for nanofluid under different operating temperatures over wedge and plate, Micromachines 13 (12) (2022), https://doi.org/10.3390/mi1312208, 2080.
[38] M. Rizwan, M. Hassan, O. Daniel, Makinde, M.M. Bhatti, M. Marin, Rheological modeling of metallic oxide nanoparticles containing non-Newtonian nanofluids and potential investigation of heat and mass flow characteristics, Nanomaterials 12 (2022) 1237, https://doi.org/10.3390/nano12071237.
[39] M. Hassan, M. Rizwan, Mathematical modeling and flow behavior of homogeneous complex MWCNT/PEG nanofluids through Burger model with Maxwell repre- representation, J. Therm. Anal. Calorim. 148 (2023) 7383–7394, https://doi.org/10.1007/s10973-023-12192-3.
[40] M. Hassan, M. Rizwan, Mathematical modeling for experimental data to investigate the convective heat transfer in non-Newtonian nanofluid's flow over a thin needle, Z. Angew. Math. Mech. 103 (9) (2023), https://doi.org/10.1002/zamm.202200344.
[41] C.L.M.H. Navier, Memory on the laws of motion of fluids, Memoires Académie des Sciences Institut de France 6 (1823) 389–416 (in French).
[42] J.C. Maxwell, On stresses in rarefied gases arising from inequalities of temperature, Philos. Trans. Royal Soc. 170 (1879) 231–256, https://doi.org/10.1098/rspl.1878.0052.
[43] A.M. Megahed, Slip flow and variable properties of viscoelastic fluid past a stretching surface embedded in a porous medium with heat generation, J. Cent. South. Univ. 23 (4) (2016) 991–999, https://doi.org/10.1007/511771-016-3147-4.
[44] Y.S. Daniel, Boundary layer stagnation point flow of a nanofluid over a permeable surface with velocity, thermal and solutal slip boundary conditions, J. Appl. Phys. Sci. Int. 4 (2015) 237–252.
[45] Y.S. Daniel, Steady MHD boundary-layer slip flow and heat transfer of nanofluid over a convectively heated of a non-linear permeable sheet, J. adv. mech. eng. 3 (2016) 1–4, https://doi.org/10.7726/jame.2016.1001.
[46] Y.S. Daniel, MHD laminar flows and heat transfer adjacent to permeable stretching sheets with partial slip condition, J. Adv. Mech. Eng 4 (2017) 1–5, https://doi.org/10.7726/jame.2017.1001.
[47] Y.S. Daniel, Z.A. Aziz, Z. Ismail, F. Salah, Effects of slip and convective conditions on MHD flow of nanofluid over a porous nonlinear stretching/shrinking sheet, Aust. J. Mech. Eng. 16 (2018) 213–229, https://doi.org/10.1080/14484846.2017.1358844.
[48] Y.S. Daniel, Z.A. Aziz, Z. Ismail, F. Salah, Slip effects on electrical unsteady MHD natural convection flow of nanofluid over a permeable shrinking sheet with thermal radiation, Eng. Lett. 26 (1) (2018).
[49] Y.S. Daniel, Z.A. Aziz, Z. Ismail, A. Bahar, F. Salah, Slip role for unsteady MHD mixed convection of nanofluid over stretching sheet with thermal radiation and electric field, Indian J. Phys. 94 (2) (2020) 195–207, https://doi.org/10.1007/s12648-019-01474-y.
[50] M. Ramzan, D.C. Jae, U. Naeem, Partial slip effect in the flow of MHD micropolar nanofluid flow due to a rotating disk-a numerical approach, Results, Phys. Met. 7 (2017) 3557–3566, https://doi.org/10.1016/j.rinp.2017.09.002.
[51] S. Nadeem, M.N. Khan, A. Nadeem, Transportation of slip effects on nanomaterial micropolar fluid flow over exponentially stretching, Alex. Eng. J. 59 (5) (2020) 3443–3450, https://doi.org/10.1016/j.aej.2020.05.024.
[52] J.A. Gbadeyan, E.O. Titiloye, A.T. Adeosun, Effect of variable thermal conductivity and viscosity on Casson nanofluid flow with convective heating and velocity slip, Heliyon 6 (1) (2020) e03076, 10.1016j.heliyon.2019.e03076.
[53] K. Ahmad, A. Ishak, M. Nazar, Micropolar fluid flow and heat transfer over a nonlinearly stretching plate with viscous dissipation, Math. Probl Eng. 1 (2013) 257161, https://doi.org/10.1155/2013/257161.
[54] E.O. Fatunmbi, A. Adeniyan, Nonlinear thermal radiation and entropy generation on steady flow of magneto-micropolar fluid passing a stretchable sheet with variable properties, R, Engage 6 (2020) 100142, https://doi.org/10.1016/j.rineng.2020.100142.
[55] C. Canuto, M.Y. Hussaini, A. Quarteroni, T.A. Zang, Spectral Methods: Fundamentals in Single Domains, Springe-Verlag Berlin Heidelberg, 2006, pp. 198–223, https://doi.org/10.1007/978-3-540-30726-6.
[56] X.Y. Tian, B.W. Li, Y.S. Wu, J.K. Zhang, Chebyshev collocation spectral method simulation for the 2D boundary layer flow and heat transfer in variable viscosity MHD fluid over a stretching plate, Int. J. Heat Mass Tran. 89 (2015) 829–837, 10.1016j.jheatmasstransfer.2015.05.102.
[57] X.Y. Tian, B.W. Li, J.K. Zhang, The effects of radiation optical properties on the unsteady 2D boundary layer MHD flow and heat transfer over a stretching plate, Int. J. Heat Mass Tran. 105 (2017) 109–123, https://doi.org/10.1016/j.ijheatmasstransfer.2016.09.060.
[58] T.G. Fang, J. Zhang, Y.F. Zhong, Boundary layer flow over a stretching sheet with variable thickness, Appl. Math. Comput. 218 (13) (2012) 7241–7252, https://doi.org/10.1016/j.amc.2011.12.094.
[59] T.G. Fang, J. Zhang, S.S. Yao, Slip MHD viscous flow over a stretching sheet–an exact solution, Commun. Nonlinear Sci. Numer. Simul. 14 (11) (2009) 3731–3737, https://doi.org/10.1016/.cnsns.2009.02.012.